Use of multifractals to detect anomalous propagation (AP) in weather radar

Dimitrios Charalampidis, Takis Kasparis, Linwood Jones, Michael Georgiopoulos
School of Electrical Engineering and Computer Science
University of Central Florida, Orlando, FL 32816

ABSTRACT

In this paper we present an automatic algorithm for the removal of echoes that are caused due to anomalous propagation (AP) from the lower radar elevation. The algorithm uses textural information as well as intensity characteristics of reflectivity maps that are obtained from the two lower radar elevations. The texture of the reflectivity maps is analyzed with the help of multifractals. We present examples that illustrate the efficiency of our algorithm. We compare our algorithm with a manual algorithm that was developed by NASA/TRMM for AP removal, in terms of total rain accumulation and in terms of the number of pixels removed.

Keywords: Multifractals, Anomalous Propagation, NEXRAD, Clutter, rainfall

1. INTRODUCTION

Geophysical systems are usually complex due to their non-linear dynamics. Several attempts to analyze these signals by their statistical properties have been made in the literature[1,2,3]. Traditional approaches include histogram analysis, examination of autocorrelation functions and energy spectra. In many cases the signal representation is in the form of an image. For instance, the images can be radar reflectivity maps, or satellite images.

Weather radars are designed to detect precipitation in the atmosphere, and echoes resulting from other sources are usually undesired. Examples of such targets are man-made structures, radar-chaff ejected by military aircraft, birds, insects, and even the earth's surface. Scattering resulting from antenna sidelobes striking the earth close-in to the radar are referred to as ground clutter. Because these objectionable echoes are at short ranges, they are easily removed in the signal processing. However, other more objectionable ground clutter may result in cases of strong vertical gradient of temperature and humidity. Here the radar beam undergoes unusual refraction and may strike the earth repeatedly for distances of hundreds of kilometers producing so called anomalous propagation (AP) while it travels.

Since AP echo intensities can exceed 60dBZ, this may create serious problems for geophysical algorithms, such as estimation of rain rate. Therefore, it is important to study the characteristics of AP so that it can be suppressed. AP suppression is the process of removing these spurious echoes from the data. This is often referred to as Quality Control (QC). Several algorithms for AP removal and rain classification have been proposed in the literature[4,5,6,7]. These algorithms are mainly based on the analysis of radar reflectivity, radial velocity as well as multifractal analysis[8,9,10,11].

Multifractals[12,13] have been proved to be useful in the analysis of complex geophysical systems[14,15]. They are based on the concept of scale invariance. Scale invariance analysis is a framework for developing statistical tools that account for all available scales at once. Scale invariance is a symmetry that is respected by systems whose large and small scales are related by a scale changing operation involving only the scale ratio. This leads to the fact that these systems do not have a characteristic scale. In multifractal analysis we seek for a power-law behavior of a partition function that is constructed from a measure, with respect to the scale parameter under consideration. If a single power-law exponent is sufficient to characterize all the statistics within a whole family, then we refer to the model as monofractal and we talk about monoscaling behavior. If more than one exponent is needed to characterize the statistical behavior of the signal then we refer to the model as multifractal and we talk about multiscaling behavior. Multifractals can be generated by different physical processes such as multiplicative cascade processes and turbulence. Self-similarity (and hence isotropy) is often assumed in scale invariant models and in analysis techniques.

In this paper we have developed an algorithm for the removal of AP from NEXRAD (Next Generation Weather Radar) images. Radar reflectivity is used for detection of AP. More specifically, reflectivity obtained from the two lower radar elevations is utilized. Rainfall and AP can not be separated using only the reflectivity intensity, since it can vary for both from negative dBz values to values greater than 60 dBZ. Since AP possesses larger variability than rainfall, the textural characteristics of reflectivity can be used in order to separate AP from useful rainfall. Even though AP echo intensities can exceed 60dBz, average rain intensities are usually stronger in a relatively large area. Our algorithm combines textural characteristics that are extracted with the help of multifractals and intensity characteristics of reflectivity in order to achieve efficient AP removal.

In cases where the goal is estimation of total accumulation, it would be sufficient for an algorithm to provide accurate information about the percentages of AP and rainfall. In such cases, specific classification of each pixel as AP or not, is not so important. In this paper we are interested in the more difficult task of detecting AP in a pixel basis which is useful in cases where the goal is radar/rain-gauge calibration, radar/satellite calibration, or even radar/radar calibration.

This paper is organized as follows: In section 2 an introduction to multifractals is presented, followed by the description of our algorithm in section 3. In section 4 we present some results and examples of AP removal. Finally in section 5 we conclude with some closing remarks.

2. MULTIFRACTAL ANALYSIS

As it was mentioned in the introduction, the scaling behavior of signals can be expressed by different scale-independent relationships. In multifractal analysis one looks for a power-law relation between a partition function that is constructed from a measure and the scale parameter under consideration. Assume that the signal studied is N-dimensional: $f(x_1, x_2,... x_N)$. One power-law relation describes the variation of the statistical moments of the measure $\mu_q(s, x_1, x_2,... x_N)$ with scale s. The measure $\mu_q(s, x_1, x_2,... x_N)$ at scale s at the location $(x_1, x_2,... x_N)$ of the N-dimensional signal is defined as:

$$\mu_q(s, x_1, x_2,... x_N) = \varepsilon_s^q (x_1, x_2,... x_N) \tag{1}$$

where

$$\varepsilon_s (x_1, x_2,... x_N) = \sum_{x_1'=x_1-s/2}^{x_1-s/2} \cdots \sum_{x_N'=x_N-s/2}^{x_N-s/2} f(x_1', x_2',... x_N') \tag{2}$$

is the sum of the function f inside a "box" of size $s \times s \times ... \times s$. The partition function is defined as the ensemble average $<\varepsilon_s^q>$ q-th moment of the signal studied. Then the power law relation is defined as:

$$< \varepsilon_s^q > \sim s^{K(q)} \tag{3}$$

The function $K(q)$ is the so called moment scaling function and characterizes the multifractal behavior of the signal f. If the function $K(q)$ is a straight line then a single power-law exponent (for instance $K(2)$) is sufficient to characterize all the statistics within a whole family and then we talk about monofractality. If the function $K(q)$ is not a straight line then more than one exponent is needed to characterize the statistical behavior of the signal and we talk about multifractality.

Practically the ensemble average $< \varepsilon_s^q >$ is approximated by the spatial average of ε_s^q under the assumption of temporal stationarity of the function f. If we consider applying the log at both sides of (3), then the function $K(q)$ is estimated

from the slope of the line that best fits the points (log s, log $<\varepsilon_s^q>$) $s = s_1, s_2,...s_L$ where s_1 is the smallest available scale and s_L is the largest available scale.

It is common instead of the function $K(q)$ to use the function $C(q)$ which is defined as:

$$C(q) = K(q)/q \tag{4}$$

3. THE AP REMOVAL ALGORITHM

The algorithm for AP removal uses the reflectivity images obtained from the two lower radar elevations. The images as they are obtained from the radar in polar coordinates but in order to simplify our analysis we transform them in Cartesian coordinates, with the radar being at the center of the image. We concentrate in AP removal for the lower elevation. Each pixel corresponds to 1 × 1 km. As it was mentioned earlier, the algorithm utilizes both textural and intensity information. Next, the algorithmic steps are presented.

3.1. Step 1: Usage of Multifractal Exponents

In the first step of the algorithm the exponents $K(q)$ or $C(q)$ are computed. We consider the reflectivity images obtained from the two lower elevations of the radar. For this step reflectivity is not considered in dBZ but in linear terms. According to the discussion in section 2, the signal under consideration is 3-dimensional. We define the measure at *scale 1*as:

$$\mu_q\,(scale\ 1,x,y,z) = [f(x,y,z)]^q \tag{5}$$

We define the measure at *scale 2* as:

$$\mu_q\,(scale\ 2,x,y) = \Big[\sum_{x'=x-1}^{x+1}\ \sum_{y'=y-1}^{y+1}\ \sum_{z'=1}^{2} f(x',y',z')\Big]^q \tag{6}$$

The coordinates (x,y,z) correspond to the pixel that exists in the (x,y) position of the z-th elevation. In order to be accurate with the definition of the measure as it is defined in (1) and (2), we should consider the fact that the radar beam widens as it travels away from the radar. The measure at each scale s is computed in a 3-dimensional "box" whose volume we need to relate with the scale s:

$$s = \sqrt[3]{V} \tag{7}$$

where V is the volume of the "box". For *scale 1* the measure $\mu_q(scale\ 1,x,y,z)$ as it is defined in equation (5) is nothing more but the reflectivity value that corresponds to the pixel with coordinates (x,y,z) raised to a power equal to q. The volume of the "box" in this case is V = 1 × 1 × A·R = A·R where R is the distance from the radar and A is a constant. Here we have assumed that the beam widens linearly with respect to R. According to equation (7) we can agree that $s = \sqrt[3]{AR}$. For *scale 2*, the volume of the "box" is 3 × 3 × 2A·R = 18 A·R. According to (7) the scale is $s = \sqrt[3]{18AR}$.

The power-law relation is the same as in equation (3). It was mentioned earlier that the function $K(q)$ is estimated from the slope of the line that best fits the points (log s, log $<\varepsilon_s^q>$). In our case s = *scale* 1, *scale* 2. According to our previous discussion the scale seems to be dependent on the distance from the radar. It is easy to show that the exponents $K(q)$ (or consecutively $C(q)$) are not. The term log (*scale 1*) can be written as log (*scale 1*) = 1/3 [log 1] + 1/3 [log A·R] and the term log (*scale 2*) can be written as log (*scale 2*) = 1/3 [log 18] + 1/3 [log A·R]. The slope of the line that best fits the points (log s, log $<\varepsilon_s^q>$) is equal to the slope of the line that best fits the points (log s + B, log $<\varepsilon_s^q>$) where B is a constant. In our case B = 1/3 [log A·R]. As a result, *scale 1* can be equivalently selected equal to 1 and *scale 2* equal to $\sqrt[3]{18}$ which are both independent of the distance from the radar.

In order to be able to separate AP from rain we need to compute the exponents $K(q)$ or $C(q)$ in small windows of the images. More specifically, the ensemble average in equation (3) is approximated with the spatial average of the measures in small 3-dimensional windows of size $w \times w \times 2$:

$$< \varepsilon_s^q >_{x,y} = (1/2w^2) \sum_{x'=x-w/2}^{x+w/2} \sum_{y'=y-w/2}^{y+w/2} \sum_{z=1}^{2} \mu_q(s,x',y',z') \quad (8)$$

for *scale 1* and:

$$< \varepsilon_s^q >_{x,y} = (1/w^2) \sum_{x'=x-w/2}^{x+w/2} \sum_{y'=y-w/2}^{y+w/2} \mu_q(s,x',y') \quad (9)$$

for *scale 2*. In equations (8) and (9) w is the length of the averaging window in the x and y directions. For instance, in Figure 1, $w = 5$.

From equations (3), (8) and (9), the exponents $K_{x,y}(q)$ are computed. Figure 1 illustrates how this step of the algorithm is implemented. A 5×5 portion of the first elevation and the corresponding 5×5 portion of the second elevation centered at locations $(x, y,1)$ and $(x, y,2)$ respectively are shown. The measures μ_q $(scale\ 1,x',y',z')$ are computed as the reflectivity values corresponding to the pixels with coordinates (x',y',z') raised to the q-th power. Then, the approximate ensemble average at location (x,y) is the average of the measure $\mu_q(scale\ 1,x',y',z')$ over all pixels for both portions. The measure μ_q $(scale\ 2,x',y')$ is computed as the reflectivity averaged in a "box" located at (x',y') which is then raised to the q-th power. One such "box" located at $(x+1,y+1)$ consists of the group of "dark gray" pixels (including the "white" pixels) as it is shown in Figure 1. Then, the approximate ensemble average at location (x,y) is the average of the measure $\mu_q(scale\ 2,x',y')$ over all (x',y').

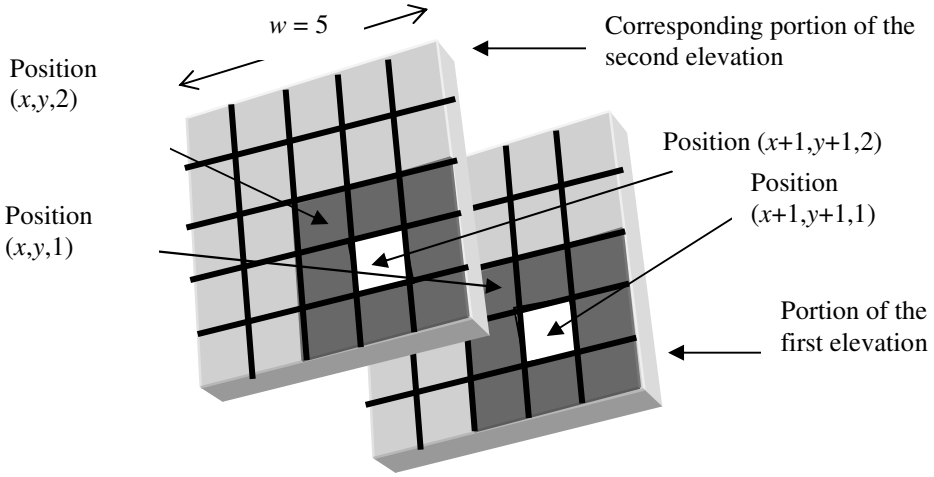

$$\mu_q\ (scale\ 1,x,y,z) = [f(x,y,z)]^q \qquad \mu_q\ (scale\ 2,x,y,z) = \sum_{x'=x-1}^{x+1} \sum_{y'=y-1}^{y+1} \sum_{z'=1}^{2} [f(x',y',z')]^q$$

Figure 1: Computation of the measures and the approximate ensemble average using the corresponding portions of the reflectivity images obtained from the two radar elevations. The "white" squares represent single pixels at locations $(x+1,y+1,1)$ and $(x+1,y+1,2)$ respectively. The group of "dark gray" squares (including the "white" squares) define a "box" at *scale 2* and at location $(x+1,y+1)$.

AP is characterized by larger variability than rain. It can be shown than larger variability, generally leads to larger $K(q)$ or $C(q)$ exponents. We have used two exponents: $Cx,y(2)$ and $Cx,y(8)$. For the computation of the approximate ensemble average we used 3-dimensional averaging windows of size $w \times w \times 2 = 8 \times 8 \times 2$. In order to reduce the variability of the two measures and to increase their robustness, we convolve each one with a two-dimensional moving average filter of size 8×8. For each of the exponents $Cx,y(2)$ and $Cx,y(8)$ we have specified a threshold (TH_1 and TH_2 respectively). If at least one of the two exponents at a location (x,y) exceeds the corresponding threshold the pixel (x,y) is characterized as an AP pixel.

3.2. Step 2: Pixel Reactivation Based on Reflectivity Intensity and Multifractal Exponents

The second step of the algorithm is applied in order to fix the problem of removing pixels that correspond to actual rainfall that occurred because of the previous step. This problem occurred because the thresholds that where applied in step 1 where relatively large, to make sure that most of the AP is removed. In this part of the algorithm we reactivate a pixel located at (x,y) of the first elevation, if the following properties hold:

1. The average intensity in dBZ in a window of size $p_1 \times p_1$ of the first elevation centered at (x,y) is larger than a specific threshold TH_1^{int} or the average intensity in dBZ in windows of size $p_2 \times p_2$ of the second elevation centered at (x,y) is larger than a specific threshold TH_2^{int}.

AND

2. The exponent $Cx,y(2)$ is smaller than a threshold $TH_1' < TH_1$ and $Cx,y(8)$ is smaller than a threshold $TH_2' < TH_2$ at the same location (x,y).

Basically, this step considers that AP has been removed, so that less strict thresholds than TH_1 and TH_2, namely TH_1' and TH_2' can be applied to the multifractal exponents. At the same time we take in account that it is not common for reflectivity corresponding to rain to have very sharp transitions. For instance it is not common to have an area with reflectivity larger than 30-40 dBZ that suddenly changes to 0dBZ. For that reason if the average intensity in dBZ in a window of size $p_1 \times p_1$ centered at pixel (x,y) of the first elevation is larger than a threshold TH_1^{int}, we reactivate this pixel (if it not already active), since it is possible that the edge of the rain has been erroneously removed in step 1. If the edges of the rain were not erroneously removed then the average in the $p_1 \times p_1$ window would be relatively small (hopefully smaller than the threshold TH_1^{int}) so that no action is taking place. Also, if p_1 is relatively large, then the probability of reactivating pixels that correspond to AP is small since it is not common for AP to have a large average reflectivity value in a relatively large area. We have selected $p_1 = 20$ and $TH_1^{int} = 25$dBZ. A similar approach is taken for the second elevation. In this case it is even less probable for AP to have large reflectivity values so that an averaging window of smaller size can be used. We have used $p_2 = 5$ and $TH_2^{int} = 20$dBZ.

We apply step 2 iteratively (three iterations) to make sure that the all pixels that correspond to rain edges are reactivated. We must note that for the averages that are mentioned in property 1 only dBZ values larger than 0 are considered.

3.3. Step 3: Final Intensity Threshold

The last step is removal of pixels located at (x,y) for which the average in dBZ in a window of size $p_3 \times p_3$ around them is smaller than a noise threshold TH_3^{int}. This step is applied to the reflectivity image obtained from the lower radar elevation. We have selected $p_3 = 3$ and $TH_3^{int} = 4$ dBZ.

4. RESULTS AND EXAMPLES

In this section we compare our algorithm with an algorithm provided by NASA/TRMM called Gvbox, in terms of rain accumulation, and in terms of the number of pixels removed. It is important to mention that it is not easy to acquire accurate information about the status of an echo (AP or rain). Even a manual algorithm such as Gvbox does not eliminate

100% of AP and does not retain 100% of rain. Sometimes this is due to the fact that the information provided is not sufficient so that it is nearly impossible even for an expert observer to distinguish AP from rain. Another reason is that the AP removal algorithm has to be applied to an enormously large number of cases so that erroneous removal of light rain or incorrect preservation of small AP areas due to overlooking is a common event.

We have selected 24 hours of NEXRAD data obtained from radar located at Melbourne Florida. We selected data from the 11th of June 99, 11 AM up to the 12th of June 99, 11 AM. This was a rainy day that included many interesting cases of AP mixed with rain. It is fairer to test our algorithm on such a day than on a day where no AP or rain occurred because the results would have been misleading. The radar performs a complete volume scan every 5 minutes so that we have 12 volume scans per hour. We are interested in the two lower elevations. The vertical angles for the two lower elevations are approximately 0.48^o and 1.4^o respectively. The reflectivity data are provided in polar coordinates (r,θ) where r is the distance from the radar and θ is the horizontal angle. The distance resolution is Δr = 1 km and the horizontal angle resolution is approximately $\Delta\theta = 0.96^o$. We consider a maximum distance from the radar r_{max} = 200 km. We transform the reflectivity maps into Cartesian coordinates, so that the reflectivity maps are in the form of images of size 400×400 pixels, where each pixel corresponds to an area of 1 km^2.

The results of the comparison between Gvbox and our algorithm are shown in Tables 1, 2, 3 and 4. In Table 1 we present the total number of pixels with corresponding reflectivity higher than specific dB levels, namely 0dB, 10dB, 20dB, 30dB, 40dB and 50dB for the unprocessed reflectivity images, the images processed with Gvbox, and the images processed with our algorithm. Table 2 presents the number of pixels with corresponding reflectivity higher than specific dB levels, that where identified as AP pixels by our algorithm and rain by Gvbox, rain by our algorithm and AP by Gvbox and rain or AP by both algorithms (agreement). In Table 3 we present the results of Table 2 but in terms of percentages with respect to the total number of pixels of the unprocessed images with corresponding reflectivity higher than specific dB levels. Finally, in Table 4 we show the total rain accumulation as it is estimated using the unprocessed images, the processed images using Gvbox and the processed images using our algorithm, for areas of 400×400 km^2 and 200×200 km^2 around the radar. For estimating the total rainfall the standard Z-R relationship $Z = 300\ R^{1.5}$ was used. Using this relationship the reflectivity Z corresponding to each pixel is transformed into rainrate R.

	Corresponding Reflectivity Larger Than:					
Number of pixels in:	**0 dB**	**10 dB**	**20 dB**	**30 dB**	**40 dB**	**50 dB**
The unprocessed images:	6417191	3742036	2385433	1180567	368183	26106
Images processed by Gvbox:	4068025	3431370	2353456	1177063	367764	26100
Images processed by our algorithm:	4291970	3462763	2355676	1176836	367677	26091

Table 1: Total number of pixels: unprocessed images, images processed by Gvbox and images processed by our algorithm

	Corresponding Reflectivity Larger Than:					
Number of pixels classified as:	**0 dB**	**10 dB**	**20 dB**	**30 dB**	**40 dB**	**50 dB**
Rain by our algorithm and as AP by Gvbox:	296431	65962	16472	6194	1794	127
AP by our algorithm and as rain by Gvbox:	71265	33396	13633	6143	1822	136
AP or Rain by both algorithms:	6049495	3642678	2355328	1168230	364567	25843

Table 2: Total number of pixels classified as: rain by our algorithm and AP by Gvbox, AP by our algorithm and rain by Gvbox, and AP or rain by both algorithms

	Corresponding Reflectivity Larger Than:					
Percentage of pixels classified as:	**0 dB**	**10 dB**	**20 dB**	**30 dB**	**40 dB**	**50 dB**
Rain by our algorithm and as AP by Gvbox:	4.6	1.8	0.7	0.5	0.5	0.5
AP by our algorithm and as rain by Gvbox:	1.1	0.9	0.6	0.5	0.5	0.5
AP or Rain by both algorithms:	94.3	97.3	98.7	99.0	99.0	99.0

Table 3: Percentage of pixels classified as: rain by our algorithm and AP by Gvbox, AP by our algorithm and rain by Gvbox, and AP or rain by both algorithms

Total Rain Accum. per km^2 (in 400×400 km^2):	mm/day	% (of rain with respect to the unproc. images)
Before processing:	1.98	100.0
After processing with Gvbox:	1.93	97.5
After processing with our algorithm:	1.94	97.8

Total Rain Accum. per km^2 (in 200×200 km^2):		
Before processing:	1.21	100.0
After processing with Gvbox:	1.09	90.4
After processing with our algorithm:	1.10	90.9

Table 4: Total accumulation estimated from the unprocessed images, from images processed By Gvbox and from the images processed by our algorithm

From the results presented in Tables 1, 2 and 3, we see that the two algorithms (Gvbox and ours) agree nicely in terms of pixels removed or retained. The two algorithms have agreed in classifying 94.3% of all pixels corresponding to positive reflectivity as either AP or rain. For pixels corresponding to reflectivity larger than 30dB, which is more important since it indicates stronger rain, the two algorithms agree by 99%.

Table 4, shows the importance of the application of an AP removal algorithm. In an area of 400×400 km^2 around the radar the rainfall percentage with respect to rainfall that was estimated from the unprocessed images, was 97.5% using Gvbox and 97.8% using our algorithm. In an area of 200×200 km^2 around the radar the rainfall percentage with respect to rainfall that was estimated from the unprocessed images, was only 90.4% using Gvbox and only 90.9% using our algorithm. These results verify that most of AP appears close to the radar.

Next, we present some examples of AP removal. In Figures 2 and 3 we present the reflectivity images obtained by the first radar elevation, the second radar elevation, the processed image using Gvbox and the image processed by our algorithm. The coordinates x=0, y=0 is where the radar is located. Figure 2 (a) illustrates an unprocessed image where AP and rain are mixed close to the radar. The region with a large density of minute spots (region approximately within coordinates x = -100 to 0 and y = -50 to 50 in Figure 2 (a)) represents AP. We notice the large variability of AP. The area of corresponding region in the second elevation is smaller, and the reflectivity values are lower as it is shown in Figure 2 (b). We notice then that the vertical reflectivity gradient is large. Figure 2 (c) shows the image processed by Gvbox and Figure 2 (d) shows the image processed by our algorithm. The processed images are similar for both algorithms. Most of the differences are related to lower reflectivity values, which indicate light rain. Furthermore, these pixels hold high uncertainty as to whether they represent rain or AP.

5. CONCLUSIONS

The proposed automated algorithm has a similar performance to the manual algorithm Gvbox provided by NASA/TRMM. Considering the labor hours that need to be dedicated to the quality control of radar images and the closeness of the results produced by Gvbox and our algorithm, we believe that the proposed algorithm is an excellent alternative for quality control. For the results presented in this paper only radar reflectivity was used. Therefore the algorithm can be used for images obtained by different types of radar as well as satellite images.

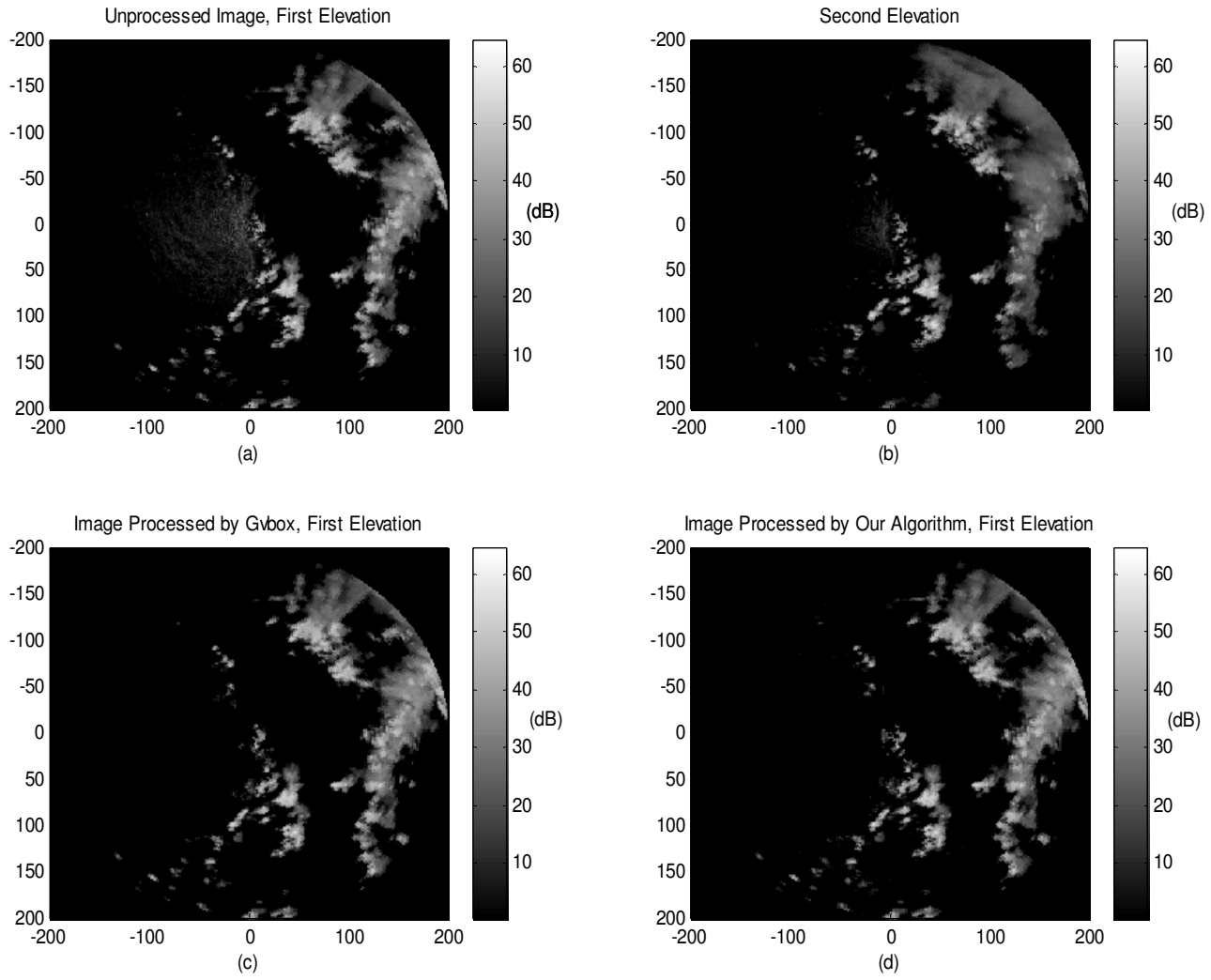

Figure 2: (a) Unprocessed image, first elevation, (b) Unprocessed image, second elevation, (c) Processed image using Gvbox, first elevation, (d) Processed images using our algorithm, first elevation.

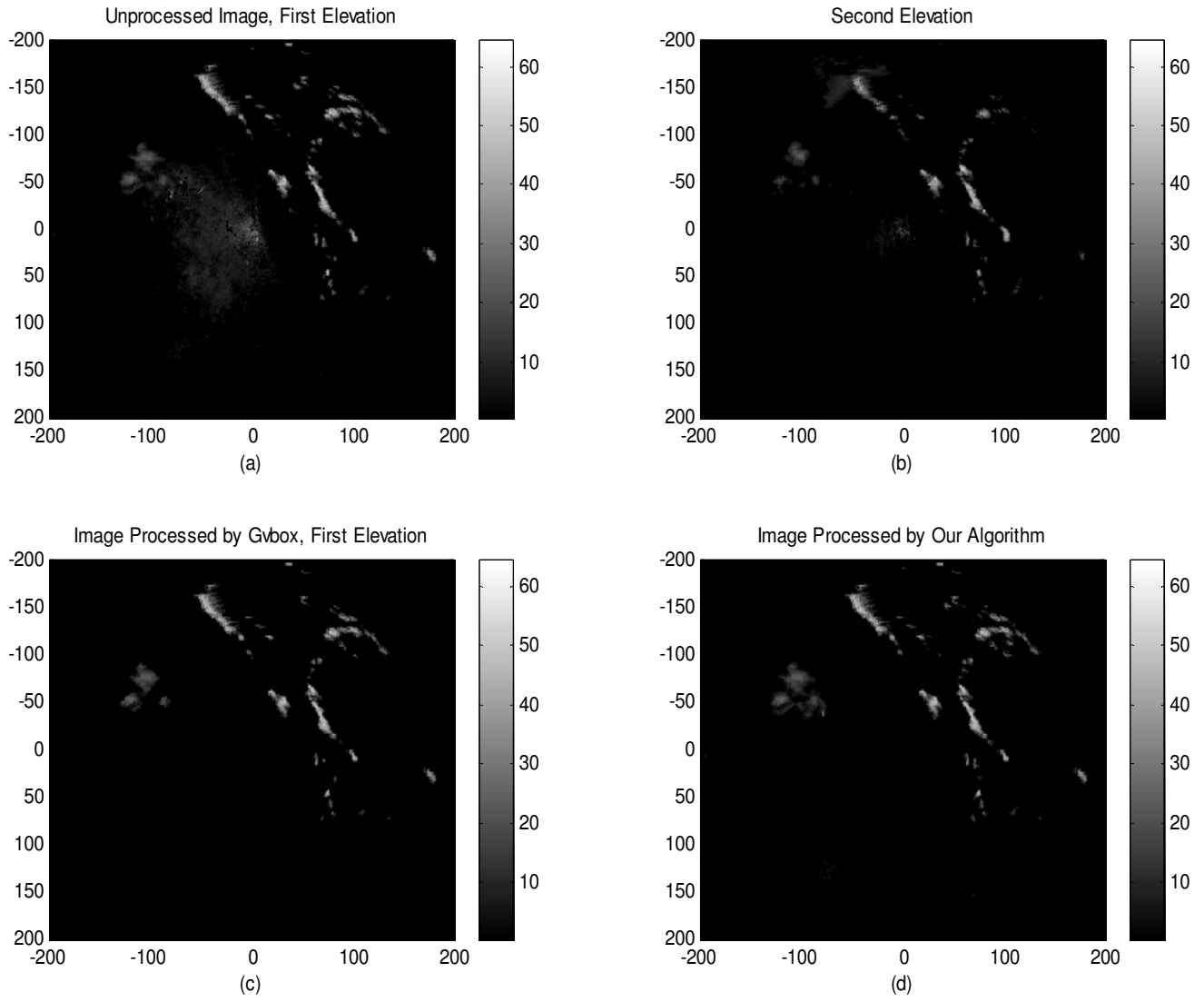

Figure 3: (a) Unprocessed image, first elevation, (b) Unprocessed image, second elevation, (c) Processed image using Gvbox, first elevation, (d) Processed images using our algorithm, first elevation.

REFERENCES

1. Q. Cheng, "Multifractality and Spatial Statistics", *Computers and Geosciences*, Vol. 25 No. 9, pp. 949-961, Nov. 1999.
2. A. Arneodo, N. Decoster, and S.G. Roux, "Intermittency, Log-Normal Statistics, and Multifractal Cascade Process in High-Resolution Sattelite Images of Cloud Structure", *Physical Review Letters*, Vol. 83, No. 6, pp. 1255 – 1259, 9 Aug. 1999.
3. V. Gupta, E. Waymire, "A Statistical Analysis of Mesoscale Rainfall as a Random Cascade", *Journal of Applied Meteorology*, pp. 251-267, Feb. 1993.

4. M. Grecu and W.F. Krajewski, "Detection of Anomalous Propagation in Weather Radar Data using Neural Networks", *IEEE Transactions on Geoscience and Remote Sensing*, Vol. 37, No. 1, pp. 287-296, Jan. 1999.
5. S. Moszkowitz, G.J. Ciach and W.F. Krajewski, "Statistical Detection of Anomalous Propagation in Radar Reflectivity Patterns", *Journal of Atmospheric and Oceanic Technology*, Vol. 11, pp. 1026-1034, Aug. 1994.
6. J.A. Pamment and B.J. Conway, "Objective Identification of Echoes Due to Anomalous Propagation in Weather Radar Data", *Journal of Atmospheric and Oceanic Technology*, Vol. 15, pp. 98-113, 1997.
7. D. Rosenfeld, E. Amitai and David Wolff, "Classification of Rain Regimes by the Three-Dimensional Properties of Reflectivity Fields", *Journal of Applied Meteorology*, Vol. 34, pp. 198-211, 1995.
8. P. Kumar, and E.F. Georgiou, "A Multicomponent Decomposition of Spatial Rainfall Fields 1. Segregation of Large- and Small-Scale Features Using Wavelet Transforms", *Water Resources Research*, Vol. 29, No. 8, pp. 2515-2532, Aug. 1993.
9. M.I.P. de Lima, J. Grasman, "Multifractal Analysis of 15-min and Daily Rainfall from a Semi-arid Region in Portugal", *Journal of Hydrology*, Vol. 220, pp. 1-11, 1999.
10. A. Mazzarella, "Multifractal Dynamic Rainfall Processes in Italy", *Theory of Applied Climatology*, Vol. 63, pp. 73-78, 1999.
11. J. Olsson, J. Niemczynowicz, "Multifractal Analysis of Daily Spatial Rainfall Distributions", *Journal of Hydrology*, Vol. 187, pp. 29-43, 1996.
12. M. Alber and Joaschim Peinke, "Improved Multifractal Box-counting Algorithm, Virtual Phase Transitions, and Negative Dimensions", *Physical Review E*, Vol. 57, No, 5, pp. 5489-5493, May 1198.
13. N. Sarkar, B.B. Chaudhuri, "Multifractal and Generalized Dimensions of Gray-Tone Digital Images", *Signal Processing*, Vol. 42, pp. 181-190, 1995.
14. M. Dekking, J.L. Vehel, E. Lutton, and C. Tricot, "Fractals: Theory and Applications in Engineering", Springer-Verlag London Limited 1999, Printed in Great Britain.
15. J. Arrault, A. Arneodo, A. Davis, and A. Marsak, "Wavelet Based Multifractal Analysis of Rough Surfaces: Application to Cloud Models and Satellite Data", *Physical Review Letters*, Vol. 79, No. 1, pp. 75-79, 7 July, 1997.